Path Integral Simulation of Charge Transfer Dynamics in Photosynthetic Reaction Centers

Eunji Sim and Nancy Makri*

School of Chemical Sciences, University of Illinois, Urbana, Illinois 61801

Received: February 26, 1997[⊗]

We present accurate path integral simulations of the primary charge separation in bacterial photosynthesis. The process is modeled in terms of the three coupled electronic states corresponding to the photoexcited special pair (the electron donor), the reduced accessory bacteriochlorophyll (the bridge), and the reduced bacteriopheophytin (the primary electron acceptor) of the L branch which interact with a dissipative medium of protein and solvent degrees of freedom. The electronic state populations are followed over 17 ps via an iterative procedure that employs a propagator functional [*Comput. Phys. Commun.* **1997**, *99*, 335]. In a previous article [*Proc. Natl. Acad. Sci. U.S.A.* **1996**, *93*, 3926] the free energy of the reduced accessory bacteriochlorophyll state and its coupling to the excited special pair were estimated by comparing the simulation results against available experimental observations on wild-type and modified reaction centers. The determined optimal parameters correspond to a simple two-step electron transfer mechanism. Additional simulations presented in this article demonstrate that the obtained parameters and the inferred mechanism are in accord with the temperature dependence of the primary charge separation and other kinetic effects observed in wild-type and modified reaction centers. We point out that the superexchange mechanism implies a large temperature effect in modified reaction centers which should be directly amenable to experimental testing. We also investigate the sensitivity of the calculated dynamics to various assumptions of the model. The results are found to be rather stable with respect to reasonable changes of the medium spectral density and the specifics of the nonequilibrium configuration o the photoexcited donor state, implying that the picture emerging from our simulations is robust and the conclusions are reliable.

I. Introduction

The first few picoseconds of photosynthesis in bacterial reaction centers involve transfer of an electron from an excited special chlorophyll pair P* (the donor) to a bacteriopheophytin on the L branch (the acceptor). In spite of the large (17 Å center-to-center) distance between these two sites,[1] the primary charge separation is characterized by a time constant of about 3 ps and a quantum yield that approaches unity. In addition, a weak inverse temperature dependence is observed. Understanding the specifics of this highly efficient electron transfer process has been the subject of numerous experimental and theoretical studies (for recent reviews see refs 2 and 3), while its mechanism has been surrounded by considerable controversy.

Because of the large separation between the primary donor and acceptor units, the corresponding electronic coupling is estimated to be very small. It is generally accepted that a bacteriochlorophyll monomer located between the special pair and the bacteriopheophytin is involved by providing a bridge state. As it is not easy to extract the energetics of the reduced bacteriochlorophyll from experiments or rigorous calculations, its role in the electron transfer process is not clear. The simplest conceivable scheme involves a two-step sequential mechanism in which the reduced bacteriochlorophyll monomer participates as a true intermediate, although its population may remain very small due to a rapid transfer to the primary electron acceptor. Another popular scenario is the superexchange mechanism in which the bridge state may enhance the transfer rate without actually accommodating the electron. Early work by Rentzepis' group established the main sequence of events in the electron transfer pathway. A series of experiments with subpicosecond resolution on the reaction centers of *Rhodopseudomonas viridis* and *Rhodobacter sphaeroides* by Holten *et al.*,[4] Woodbury *et al.*,[5] Martin *et al.*,[6] Breton *et al.*,[7−9] and Fleming *et al.*[10,11] determined the kinetic features of the primary charge separation and its temperature dependence. As no reduced bacteriochlorophyll transient was detected in these experiments, these studies concluded that the electron transfer proceeds via superexchange or by a sequential mechanism whose second step is considerably faster than the first. Recent experiments on various modified reaction centers of *Rb. sphaeroides* by Zinth's group have reported substantial long-lived population of the bridge state,[12,13] indicative of a two-step transfer. However, it has been argued that the presence of a long-lived reduced bacteriochlorophyll intermediate is not sufficient to rule out the superexchange hypopthesis and that a large bridge population may result even if that state has energy much higher than that of the electron donor.[14]

Until recently, most theoretical work on the mechanism of primary charge separation focused on estimating the free energy of the reduced accessory bacteriochlorophyll and its coupling to donor and acceptor from available experimental data[15−18] and also by means of semiempirical electronic structure calculations.[19−25] The large spread of the resulting bridge free energy values, which appear rather sensitive to details of the model employed in each calculation, evoked further the controversy about the electron transfer mechanism. Creighton *et al.* employed a quasiclassical trajectory model[21] to show that the two-step mechanism is preferred with their calculated free energy values, although superexchange could become dominant if the calculated parameters were varied within the estimated error bars. Hu and Mukamel used a perturbative density matrix treatment to explore the contributions of the sequential and superexchange mechanisms.[26,27] Using nonadiabatic electron

[⊗] Abstract published in *Advance ACS Abstracts,* May 1, 1997.

S1089-5647(97)00707-4 CCC: $14.00

transfer theory, Bixon *et al*. proposed that both mechanisms contribute to the process.[16] More recently, Egger and Mak used quantum Monte Carlo path integral methods to simulate the initial 2 ps of the process modeled as a three-state system coupled to a harmonic bath of ohmic spectral density.[28,29] By exploring various parameter combinations, these authors concluded that dynamics compatible with the experimental findings on wild-type reaction centers can arise if the reduced accessory bacteriochlorophyll lies about 600 cm^{-1} below or above the photoexcited special pair. However, that study arbitrarily restricted the ratio of electronic couplings, leading to rejection of otherwise acceptable parameters; in addition, the simulation time was generally too short to establish the maximum height of the transient bridge population and its survival time, and no definitive conclusions could be drawn.

In a recent article[30] Makri *et al*. presented accurate path integral calculations on a three-state model of charge transfer in wild-type and modified photosynthetic reaction centers using spectral densities obtained from large-scale molecular dynamics simulations.[24] The scheme employed in that work[31,32] does not suffer from phase cancellation problems typical of real-time Monte Carlo path integral methods and thus allowed calculation of the electronic state dynamics over 17 ps; this time interval is sufficiently long for transient populations to decay, offering a complete and unambiguous picture of the process. The above simulations concluded that the detection of a significant long-lived population of the reduced chlorophyll monomer is not compatible with a superexchange mechanism, although non-negligible transient population of this state can build up if the bridge lies up to a few hundred wavenumbers above the excited special pair. Thus, agreement with the observation reported in ref 12 is possible only via a two-step mechanism involving a low-lying bridge state, while comparison with the kinetic data of refs 6−8 leads to estimates for the electronic couplings in the native species. Recent calculation by Zhang and Friesner of these couplings by means of *ab initio* electronic structure methods[33] resulted in values that are in very good agreement with those determined from the path integral simulations of Makri *et al*.

Accurate evaluation of the path integral for systems in sluggish, strongly dissipative media over long simulation times is possible via an iterative procedure that employs a *propagator functional*.[32] This scheme exploits the finite length of nonlocal interactions in the influence functional for condensed phase environments.[34] The evolution is calculated iteratively with the aid of a propagator functional whose components are statistically significant paths of length equal to the range of nonlocality. The iterative procedure circumvents the phase cancellation problem and leads to stable, yet accurate results over long time intervals.

In the present paper we present a more elaborate study of the electron transfer process in bacterial photosynthesis. Specifically, we investigate the implications of the sequential model with our optimal parameters for the dependence of the electron transfer rate on temperature and on the kinetic effects caused by various chemical modifications introduced in recent studies. The results of these calculations compare well with the corresponding experimental observations, offering further support for the sequential mechanism. In addition, we explore the sensitivity of the dynamics with respect to various parameters and assumptions of the model, including the precise form of the initial unrelaxed state of the protein environment. We find that the results of our dynamics calculations are largely insensitive to variation of the parameters, confirming that the model is robust and the conclusions meaningful.

Section II describes the three-state electron transfer model that we employ. The iterative path integral scheme that we use is reviewed in section III. The same section illustrates the implementation of that scheme on the present system and discusses its convergence characteristics. Our simulation results are presented in section IV. Comparison of these results with experimental data on wild-type and modified reaction centers helps establish the energetics of this system. That section also presents the temperature dependence of the calculated electron transfer rate and explores the sensitivity of the simulation results to the medium spectral density and the assumed initial protein state. In addition, further kinetic experiments are proposed that should offer additional information on the charge transfer mechanism. Finally, section V discusses these findings, showing that they are compatible with a sequential mechanism, and concludes with brief remarks.

II. The Model

A. Electronic Hamiltonian and Protein Environment. We model the primary charge separation in terms of the three most relevant electronic states. The process starts with photoexcitation of the special bacteriochlorophyll pair P. The primary charge separation is concluded with transfer of an electron to the bacteriopheophytin H_L (see Figure 1). The transfer is mediated by the bacteriochlorophyll monomer B_L, whose reduced state couples to the electronic states of donor and acceptor. We adopt the following abbreviated notation for these states.

State 1: $P^*B_L H_L$ (donor)

State 2: $P^{*+}B_L^- H_L$ (bridge)

State 3: $P^{*+}B_L H_L^-$ (acceptor)

Ignoring direct donor−acceptor coupling, which is estimated to be very small due to the large separation of these units, the Hamiltonian matrix for these states takes the following form:

$$H_0 = \begin{pmatrix} E_1 & V_{12} & 0 \\ V_{12} & E_2 & V_{23} \\ 0 & V_{23} & E_3 \end{pmatrix} \tag{2.1}$$

Here E_i denote the free energies of the three electronic states defined above and V_{ij} are the electronic couplings responsible for charge transfer.

The above Hamiltonian describes the energetics with all nuclear coordinates frozen at the minima of the corresponding diabatic potential curves. However, the charge transfer is strongly affected by the nuclear motion of the protein and water environment. Because of the long-range nature of the Coulomb potential, a large number of protein and solvent coordinates are involved and the role of the medium is believed to be equivalent to that of a Gaussian heat bath.[35−40] Warshel and co-workers have pioneered the use of classical simulation methods for mapping anharmonic solvents onto effective harmonic oscillator baths by means of inverting energy gap correlation functions[41,42] and investigated the deviations of the free energy surfaces from the quadratic form.[60]

In the absence of more specific information, we assume that the minimum energy configurations of these states lie on a straight line, being separated by equal distances, and that the frequencies and coupling characteristics of the effective medium modes have the same values for all three states. Nonlinear arrangements of a donor−acceptor electron transfer pair with respect to an electronic ground state have been considered by

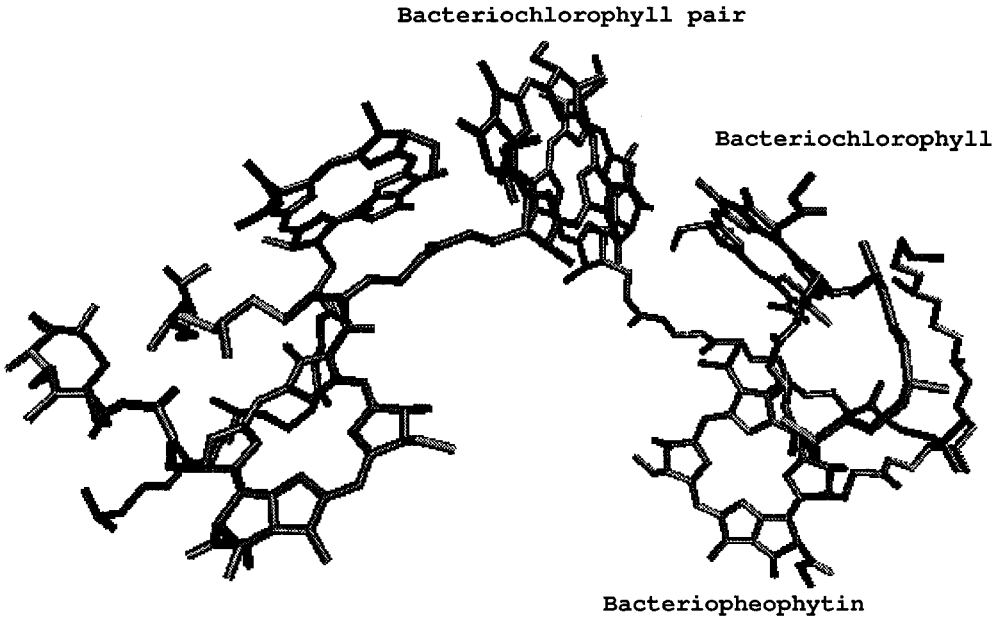

Figure 1. Arrangement of chromophores in the photosynthetic reaction center of *Rb. sphaeroides*. The center-to-center distance between the bacteriochlorophyll special pair (donor) and the bacteriopheophytin (acceptor) is 17 Å.

Cho and Silbey,[43] who explored the consequences of nonequilibrium preparation resulting from a vertical excitation. A similar formulation of the present problem would be extremely complicated, as one would have to account for nonplanar arrangements of the four relevant electronic states. We note that nonequilibrium initial state effects were found to be largest in linear arrangements,[43] and thus the behaviors observed in our linear model provide a good estimate of the sensitivity of our results to the initial preparation of the system.

The above assumption for the configuration of the electron transfer states in the three-state model of the primary charge separation in contact with a Gaussian medium leads to the following Hamiltonian:

$$H = H_0 + \sum_j \frac{p_j^2}{2m_j} + \frac{1}{2}m_j\omega_j^2\left(x_j - \frac{c_j}{m_j\omega_j^2}\mathbf{d}\right)^2 \quad (2.2a)$$

where

$$\mathbf{d} = \begin{pmatrix} -\delta & 0 & 0 \\ 0 & 1-\delta & 0 \\ 0 & 0 & 2-\delta \end{pmatrix} \quad (2.2b)$$

Here δ is an auxiliary parameter that allows us to consider unrelaxed initial states of the bath. We adopt the convention that the electronic ground state and thus the protein and solvent modes of the excited complex are initially in the equilibrium state of a multidimensional parabolic potential centered about $x_j = 0$. Then, by setting $\delta = 0$ our model describes an initial state where all nuclear coordinates are equilibrated with respect to state 1, i.e. with the excited special pair. Nonzero values of δ correspond to nonequilibrium initial states of the medium where the nuclear coordinates are displaced, as in photoexcitation achieved by means of a vertical transition from the ground state P when the latter is displaced with respect to P*.[43] The solvation energy E_s of the initial state is determined from the fluorescence Stokes shift. Typical arrangements of these states are depicted in Figure 2.

The individual frequencies and coupling constants of the harmonic bath modes need not be specified explicitly. It can be shown that the effects of a harmonic bath on the electron transfer dynamics can be expressed in terms of the bath response function[44]

$$\alpha(t) = \frac{1}{\hbar}\sum_j c_j^2 \langle x_j(0)\, x_j(t)\rangle_\beta \quad (2.3)$$

where $x_j(t)$ denotes the Heisenberg operator for the position variable of the jth bath oscillator and the brackets denote the canonical average at temperature $1/k_B\beta$. In turn, this function can be expressed in terms of the bath spectral density[45]

$$J(\omega) = \frac{\pi}{2}\sum_j \frac{c_j^2}{m_j\omega_j}\delta(\omega - \omega_j) \quad (2.4)$$

through the relation

$$\alpha(t) = \frac{1}{\pi}\int_0^\infty d\omega\, J(\omega)\left(\coth\left(\frac{1}{2}\hbar\omega\beta\right)\cos(\omega t) - i\sin(\omega t)\right) \quad (2.5)$$

We specify these collective characteristics of the bath by employing classical trajectory simulations and invoking the quantum-classical correspondence for harmonic oscillators. Specifically, as the nuclear degrees of freedom (modeled as classical variables) fluctuate about their equilibrium configuration, the energy gap between the donor and acceptor states fluctuates as the function

$$\text{const} + 2\sum_j c_j x_j^{cl}(t)$$

where $x_j^{cl}(t)$ denote classical coordinates. The correlation function $C_{13}(t)$ of the donor−acceptor energy gap fluctuations about its equilibrium average is thus equal to

$$C_{13}(t) = 4\sum_j c_j^2\langle x_j(0)\, x_j(t)\rangle_\beta^{cl} \quad (2.6a)$$

where the superscript indicates the classical position correlation function of the medium. Noting that $C_{13}(t)$ is simply related to

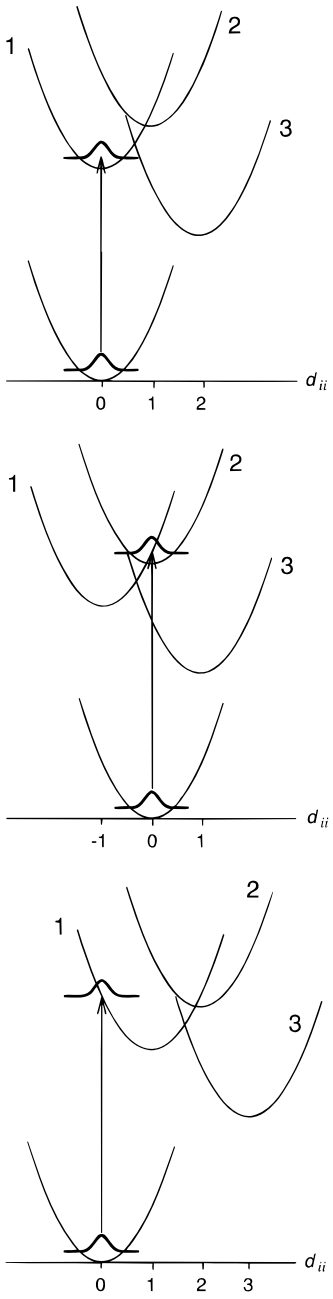

Figure 2. Schematic representation of the diabatic free energy surfaces in the linear model discussed in section II. Three configurations of the electronic ground state of the bacteriochlorophyll special pair are shown, resulting in different initial states. (a) No displacement ($\delta = 0$), resulting in an excited state at thermal equilibrium. (b) No displaced toward the bridge ($\delta = 1$); the solvation energy of the initial donor state is $E_s = E_r/4$. (c) The ground state is displaced away from the bridge ($\delta = -1$); the solvation energy of the initial donor state is $E_s = E_r/4$.

the classical limit of the response function,

$$C_{13}(t) = 4 \lim_{\hbar \to 0} \hbar\alpha(t) \tag{2.6b}$$

the gap fluctuation correlation function can be expressed in terms of the spectral density according to the relation

$$C_{13}(t) = \frac{8}{\pi\beta} \int_0^\infty \frac{J(\omega)}{\omega} \cos \omega t \, d\omega \tag{2.7}$$

which can be inverted to yield the spectral density as the Fourier integral

$$J(\omega) = \frac{\omega\beta}{4} \int_0^\infty C_{13}(t) \cos \omega t \, dt \tag{2.8}$$

Finally, the energy E_r for reorganization of the bath between the primary electron donor and acceptor states is given from the relation

$$E_r = \frac{4}{\pi} \int_0^\infty \frac{J(\omega)}{\omega} d\omega \tag{2.9}$$

while the reorganization energy between donor and bridge (and also that between bridge and acceptor) is equal to $E_r/4$.

B. Parameters. In section IV we present path integral results on the dynamics of electron transfer in the wild-type and modified reaction centers of *Rb. sphaeroides*. The pigments of these systems are specified in Table 1. We set $E_1 = 0$ in all cases. The value of E_3 is determined from magnetic experiments and known redox potentials[12,46,47] and is shown in Table 1 for the various systems studied. The free energy of the accessory chlorophyll is varied in the range -600 to $+2000$ cm^{-1}, the first of these values being a lower bound implied by the experimental data reported in ref 12 (see also section IVA.2). Similarly, the electronic couplings V_{12} and V_{23} are varied. For each set of these three unknown parameters the electron transfer dynamics are calculated over a time interval sufficiently long to determine rates and population characteristics. Comparison with various experimental findings serves as the acceptance criterion for realizable parameters.

From the weak temperature dependence of the experimental transfer rate in wild-type reaction centers[10] it is concluded that the rate-determining step is nearly activationless. With large positive values of the bridge free energy, for which the dominant mechanism is superexchange, activationless transfer implies that the reorganization energy between donor and acceptor must coincide with the donor−acceptor energy gap, i.e., $E_r \approx E_1 - E_3$. On the other hand, with values of E_2 slightly below E_1 the process is sequential and the small population of the bridge state implies that $P^*B_L H_L \rightarrow P^{*+}B_L^- H_L$ is the rate-determining step. In this case the reorganization energy between donor and bridge must be approximately equal to the energy gap of these states, i.e., $E_r/4 = E_1 - E_2$. The calculations presented in section IV use the value $E_r = 2000$ cm^{-1}. This satisfies the above requirement for the wild-type reaction centers if $E_2 \gg 0$, in which case superexchange dominates, and also with $E_2 \approx -500$ cm^{-1}, for which the transfer is sequential. For intermediate values of the bridge free energy the above choice of reorganization energy is not optimal; however, we have verified that it does not affect qualitatively the population characteristics on which our conclusions are based.

As discussed earlier, photoexcitation of the special chlorophyll pair produces a nonequilibrium state where the protein and solvent modes may possess a significant amount of excess vibrational energy arising from the vertical transition from a displaced ground state. Most of the simulations in section IV use the value $E_s = 500$ cm^{-1}, which is estimated from the measured Stokes shift.[48] Since 500 cm^{-1} $= E_r/4$, the above solvation energy corresponds to $\delta = \pm 1$ in the notation of eq 2.2 (see Figure 2). As the assumed linear arrangement possibly overestimates the effects of the initial nonequilibrium preparation,[43] we also perform simulations with smaller values of E_s. These simulations show that our results are qualitatively insensitive to details of initial preparation.

Using their dispersed polaron model, Warshel *et al.* have calculated energy gap correlation functions for the donor−bridge pair[59] and extracted spectral densities for this kinetic step. Spectral densities for the primary charge separation have also

TABLE 1: Characterization of Reaction Centers Considered in This Article; Free Energies Are Given Relative to the Energy of the Primary Electron Donor State

	wild type	modified reaction center M1	β mutant	double mutant M2
bridge chromophore	bacteriochlorophyll	bacteriochlorophyll	bacteriochlorophyll	bacteriochlorophyll with Asp
electron acceptor	bacteriopheophytin	pheophytin	bacteriochlorophyll	bacteriochlorophyll
E_3	-2000 cm^{-1}	-630 cm^{-1}	E_2 of wild type	E_2 of wild type

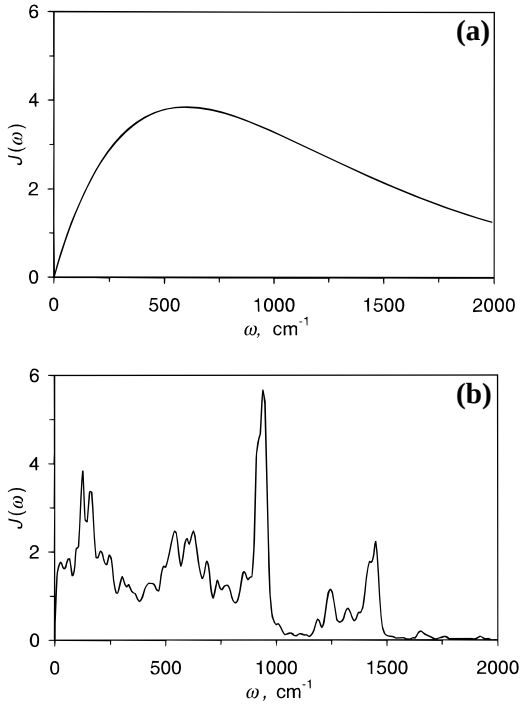

Figure 3. Spectral densities employed in the quantum simulations described in section II. (a) SD1, obtained from an ohmic fit to the spectral density of model I in ref 24. (b) SD2, obtained from model II of the same work. See the text for details.

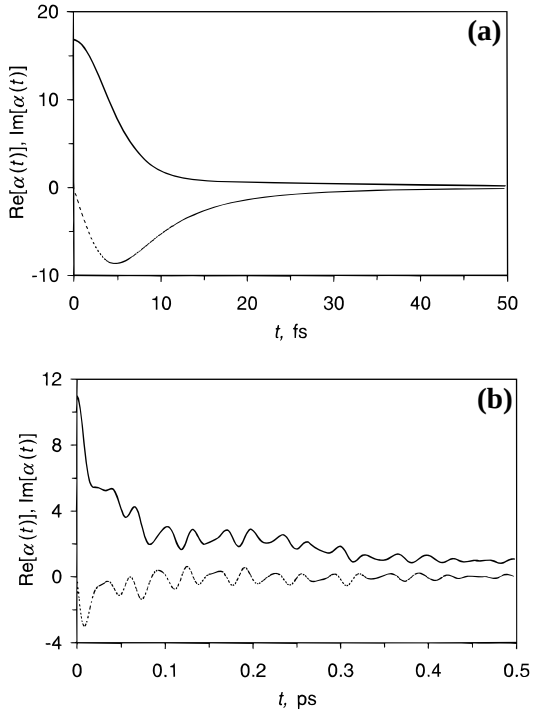

Figure 4. Bath response functions $\alpha(t)$ defined in eq 2.5 at 300 K for the two spectral densities depicted in Figure 3. (a) Response function obtained from SD1. (b) Response function obtained from SD2. Solid and dotted lines correspond to real and imaginary parts of these functions, respectively.

been calculated by Schulten and Tesch,[49] as well as by Chandler and co-workers[24] via molecular dynamics simulations on *Rps. viridis*. The gap fluctuation correlation functions obtained from these simulations differ primarily in their behavior at long times. The correlation function of Schulten and Tesch decays approximately exponentially, with a time constant equal to 94 fs, while small amplitude correlations that persist for several picoseconds emerged from the simulations of Chandler's group.

Our simulations employ two spectral densities that correspond to different parametrizations in the work of Marchi *et al.*[24] The first (hereafter SD1) was obtained from an approximate fit of ohmic form,

$$J(\omega) = \frac{\pi\hbar\alpha}{2}\omega e^{-\omega/\omega_c} \tag{2.10}$$

with $\alpha = 1.67$ and $\omega_c = 600$ cm^{-1}, to the spectral density of model I in ref 24 which was obtained by molecular dynamics with the CHARMm force fields but omitted crystallization water. The second spectral density (abbreviated SD2) is the one calculated from the molecular dynamics simulation with model II in the same work, which included crystallization water molecules treated as simple point charges. These spectral densities are depicted in Figure 3. It is seen that SD2, which is considered the more realistic of these two spectral densities, weighs low frequencies more heavily than SD1. Naturally, none of these spectral densities are quantitatively accurate at very small frequencies, which correspond to the long time (tens of picoseconds) tail of the gap correlation function. Such frequencies have been estimated to account for a considerable fraction of the total reorganization energy[50] and have been shown to result in deviations from exponential kinetics.[51] Although our simulations that employ these spectral densities may be missing some degree of nonexponential behavior in each kinetic step, we believe that the neglect of very low frequency modes not captured in SD2 does not impact on our conclusions, which are drawn from bulk features of the electronic population dynamics.

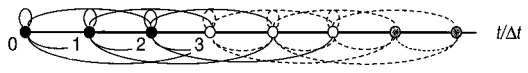

Figure 5. Diagrammatic representations of the path integral interactions in a case where the memory length is equal to three time steps. The reduced density matrix functional at $t = 0$ consists of statistically significant paths specified by the time points shown as solid circles.

The bath response functions corresponding to these spectral densities are shown in Figure 4. As expected, the lower frequency features of SD2 result in slow decay of the corresponding response function, introducing long memory correlations in the path integral calculation.

III. Filtered Propagator Functional

A. The Method. We calculate the quantum dynamics of the three coupled electronic states in contact with a dissipative medium of sluggish protein and solvent modes characterized by a spectral density of the type shown in Figure 3 with the filtered propagator functional (FPF) methodology,[32] which amounts to an iterative evaluation of the path integral. In this method, an extended reduced density functional **R** of statistically

significant electronic path segments with time span given by the correlation time of the environment[34,52,53] is propagated forward in time by means of a restricted functional integral[54] involving a dissipative propagator functional **T**. In the discrete time representation, where Δt is the elementary time step employed in the propagator and the medium effective correlation time corresponds to Δk_{max} time steps of length Δt, the procedure reduces to the following matrix−vector multiplication:

$$\mathbf{R}((n+1)\Delta k_{max}\,\Delta t) = \mathbf{T}\cdot\mathbf{R}(n\Delta k_{max}\,\Delta t) \qquad (3.1)$$

where **R** is an array of L statistically significant forward and backward path segments $(\sigma_1^{\pm}, \sigma_2^{\pm}, ..., \sigma_{\Delta k_{max}}^{\pm})_i$, $\sigma_{\pm}^k = \{-\delta, 1-\delta, 2-\delta\}$ being the electronic state index and **T** the propagator matrix in the quasiadiabatic propagator discretization of the path integral[53,55] given explicitly in ref 32. The electronic reduced density matrix $\tilde{\rho}$ is obtained from the relation

$$\tilde{\rho}((n+1)\Delta k_{max}\,\Delta t) = \mathbf{T}_{end}\cdot\mathbf{R}(n\Delta k_{max}\,\Delta t)$$

where $\mathbf{T}_{end}$ is the end-point propagator defined in ref 32. The diagonal elements $\tilde{\rho}_{ii}$ of the reduced density matrix correspond to populations of the three diabatic electronic states and are denoted as P_i.

Statistically significant path segments are selected via a Monte Carlo random walk according to their weight (absolute value) in a modified path integral expression for the reduced density matrix at total time $\Delta k_{max}\,\Delta t$ where the electronic system initial density matrix is replaced by unity.[31] Efficient sampling is achieved with the aid of a modified sampling procedure where a random number m of consecutive electronic coordinates σ_{k+1}, σ_{k+2}, ..., σ_{k+m} in a forward or backward path are incremented simultaneously in each step.

B. Convergence Characteristics. With the quasiadiabatic splitting of the propagator, converged results for the Hamiltonian of eq 2.2 are obtained with time step Δt that (depending on the various parameters considered in section IV) ranges between 3 and 13 fs.

SD2 corresponds to a fairly long correlation length and requires values of Δk_{max} up to 35 for convergence. The number L of statistically significant paths varies substantially, depending on the bridge free energy and the coupling strengths; the results shown in the next section were obtained with L in the range 10^4-10^5. Omission of small-weight path segments leads to deviations of the norm from unity; that is, the trace of the reduced density matrix is conserved only approximately, $\sum_{i=1}^{3} \tilde{\rho}_{ii}(t) \approx 1$. The magnitude of these deviations from rigorous norm conservation provides a useful measure of the numerical accuracy of the calculation.[32] Typically, the results presented in section IV conserve the norm (and thus are converged) within 5%.

Through a series of calculations where the memory $\tau_m = \Delta k_{max}\,\Delta t$ included in the propagator functional is kept fixed, we have estimated the maximum time step Δt allowed for each set of parameters. To determine the required memory length τ_m we varied Δk_{max}, keeping Δt fixed, until convergence was reached. As a simple illustration of the FPF convergence characteristics in the case of the problem at hand we present simulation results for two typical configurations as a function of the memory included explicitly in the path integral. Figure 6a,b shows the time evolution of two electronic states populations, along with the calculated trace of the reduced density matrix, as functions of the total memory length included in the propagator functional for the two spectral densities described in section II. In all cases the normalization is fairly close to unity and we estimate the error incurred due to path filtering to be smaller than 5%. From this illustrative example the effective range τ_m of nonlocal interactions appears to be about 20 fs in the case of SD1, while $\tau_m \approx 0.33$ ps if SD2 is used. Thus, as expected on the basis of the response functions presented in section II, inclusion of much longer memory interactions is indeed necessary in the case of the lower frequency SD2. We also note that the results obtained in the case of SD2 with $\tau_m =$ 0.132 and 0.198 ps, although not converged, are in this case accidentally close to one another. Such behavior is caused by the distinctive features of SD2, which lead to long-ranged oscillatory patterns in the corresponding response function. Convergence is eventually achieved with $\tau_m = 0.33$ ps, which corresponds to $\Delta k_{max} = 25$ with the optimal time step $\Delta t =$ 13.2 fs, as concluded from test calculations with even longer memory not shown in Figure 6b.

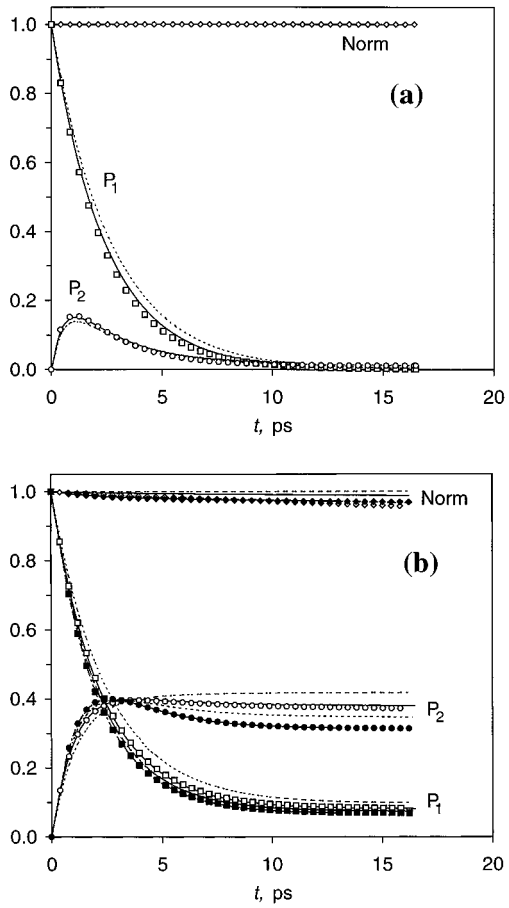

Figure 6. Convergence of the FPF scheme with respect to the total memory $\tau_m = \Delta k_{max}\,\Delta t$ included in the propagator at 300 K. Shown are the populations P_1 and P_2 of the photoexcited special pair and the reduced accessory bacteriochlorophyll states, as well as the norm $\sum_{i=1}^{3} P_i$. (a) Wild-type reaction center with SD1 and the parameters $E_2 = -400$ cm^{-1}, $V_{12} = 22$ cm^{-1}, $V_{23} = 135$ cm^{-1}, and $\Delta t = 5$ fs. The solvation energy of the initial state is $E_s = 500$ cm^{-1} ($\delta = 1$). Dashed lines, solid lines, and markers correspond to $\Delta k_{max} = 3$, 4, and 5, respectively. (b) Mutant M1 and SD2 and the parameters $E_2 = -400$ cm^{-1}, $V_{12} = V_{23} = 22$ cm^{-1}, and $\Delta t = 13.2$ fs. Dashed lines: $\Delta k_{max} = 5$. Solid lines: $\Delta k_{max} = 10$. Hollow markers: $\Delta k_{max} = 15$. Dotted lines: $\Delta k_{max} = 20$. Dash-dotted lines: $\Delta k_{max} = 25$. (These lines are not discerned easily, as they essentially coincide with the solid markers.) Solid markers: $\Delta k_{max} = 30$.

IV. Results

Our principal goal is estimating the appropriate parameter sets E_2, V_{12}, and V_{23}, which give results compatible with experimental data, in order to shed light onto the electron transfer mechanism. In an earlier publication[54] we pursued this

TABLE 2: Configurations (Free Energies and Coupling Constants) Explored in Section IV; All Values Are in cm^{-1}

system	configuration	E_2	E_3	V_{12}	V_{23}
wild type	C1	−400	−2000	22	90
wild type	C2	−400	−2000	22	135
modified reaction center M1	C3	−400	−630	22	22
modified reaction center M1	C4	+200	−630	30	30
modified reaction center M1	C5	+500	−630	60	60
modified reaction center M1	C6	+2000	−630	240	240
double mutant M2	C7	+500	−400	22	135

goal by fitting the computed population dynamics to available kinetic data from wild-type reaction centers[4−10] and a modified species where detection of a B_L^- intermediate was reported for the first time.[12,13] Our calculations led to the conclusion that the primary charge separation is a two-step process. Here we present a more detailed study, exploring the sensitivity of our earlier conclusions with respect to various assumptions of the model and assessing the implications of our optimized parameters with regard to other experimental facts. For this purpose we compare the population dynamics and the temperature dependence of the electron transfer rate in various systems with our simulation results. We also propose kinetic experiments which should offer further verification of the sequential mechanism. In view of the simplicity of our three-state model, the comparisons presented below focus on the qualitative rather than quantitative trends induced by variation of structural or environmental factors.

In part A of this section we present numerical simulations at room temperature on wild-type and modified reaction centers with various energy and coupling parameters displayed in Table 2 using both spectral densities and compare the results with those from available experiments. These calculations employ an unrelaxed initial state displaced in the direction of the reduced accessory chlorophyll (cf. Figure 2b) with the solvation energy $E_s = 500$ cm^{-1}. Part B presents simulations at lower temperatures for several parameter sets. Finally, in part C we discuss the sensitivity of the results with respect to the solvation energy and displacement of the initial protein state and show that the population characteristics are qualitatively insensitive to reasonable uncertainties in the preparation of the system.

A. Population Kinetics at Room Temperature. *1. Wild-Type Reaction Center.* For wild-type reaction centers, time-resolved spectroscopy experiments by Martin and co-workers[6−8] have shown that the time constant of the electron transfer from donor to acceptor is about 3 ps. In this case bridge population is difficult to detect and thus is presumed to be small and short-lived.

The donor−acceptor energy gap $E_1 - E_3$ in wild-type reaction centers is known to be about 2000 cm^{-1}.[46,47] Recent experiments[12] (see below) observe approximately 0.7 population transfer to the primary electron acceptor in a modified reaction center where $E_3 \approx -630$ cm^{-1}, thus placing a lower bound on the value of the bridge free energy.

Our simulations indicate that any value of the bridge free energy greater than the above bound can with appropriate electronic couplings give rise to populations consistent with those observed in the time-resolved experiments described above. This conclusion differs from that reached by Mak and Egger,[28,29] whose simulations arbitrarily restricted the relative magnitude of the electronic coupling strengths. With large positive values of E_2 both electronic couplings must be large (10^2−10^3 cm^{-1}) in order to reproduce the observed time constant of 3 ps. For low-lying bridge configurations and if indeed the solvation energy of the initial protein unrelaxed state is non-

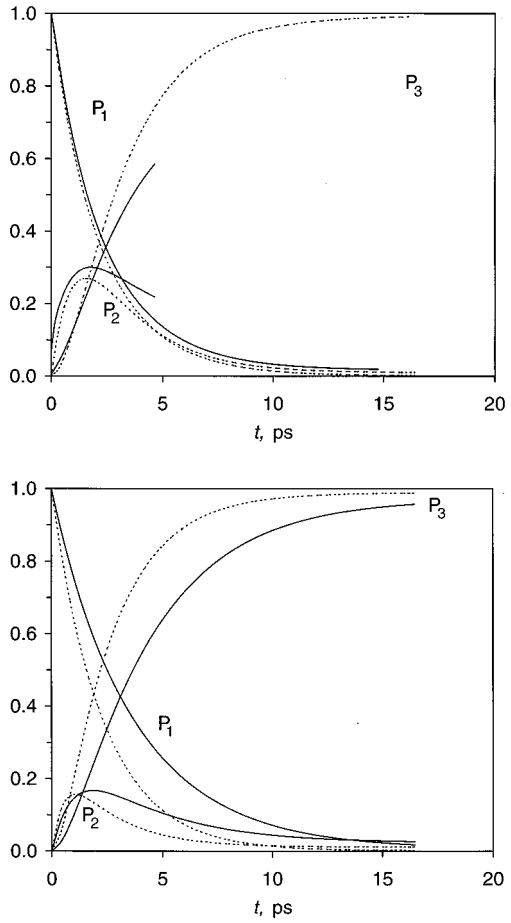

Figure 7. Evolution of the electronic state populations for the wild-type reaction center with the parameters $E_2 = -400$ cm^{-1}, $E_3 = -2000$ cm^{-1}, and $V_{12} = 22$ cm^{-1}. The solvation energy of the initial state is $E_s = 500$ cm^{-1} ($\delta = 1$). Dashed and solid lines correspond to SD1 and SD2, respectively. All results shown are converged to 5%. (a) $V_{23} = 90$ cm^{-1}. (b) $V_{23} = 135$ cm^{-1}.

negligible, the bridge−acceptor coupling V_{23} must be significantly larger than V_{12} to prevent transient buildup of population on the accessory chlorophyll above the experimental detection threshold. This behavior is illustrated in Figure 7a,b, which shows the evolution of the electronic populations with the configurations C1 and C2, respectively, both of which use the bridge free energy $E_2 = -400$ cm^{-1} and an initial state shifted toward the bridge with solvation energy equal to 500 cm^{-1}. Both spectral densities produce qualitatively similar results. The value $E_2 = -400$ cm^{-1} corresponds to the "optimal" configuration as determined from simulations discussed in the next subsection. The chosen magnitude of the donor−bridge electronic coupling $V_{12} = 22$ cm^{-1} adjusts the time constant of the rate-determining donor−bridge step to the value measured by Martin and co-workers.[6−8] Although the magnitude of the second electronic coupling has little effect on the observed kinetics, it is seen to control the transient bridge population. As discussed in the earlier work by Makri *et al.*,[54] our simulations set the value $V_{23} = 135$ cm^{-1} as a lower limit for that coupling in order for P_2 to remain below 0.15 at all times. Recent *ab initio* electronic structure calculations by Zhang and Friesner[33] obtained the values 17 and 122 cm^{-1} for V_{12} and V_{23}, respectively, in excellent agreement with our earlier estimates.

2. Reaction Centers with Modified Acceptor Pigments. Various chemical modifications have been introduced by several experimental groups in order to elucidate the mechanism of the primary charge separation. Holten and co-workers have re-

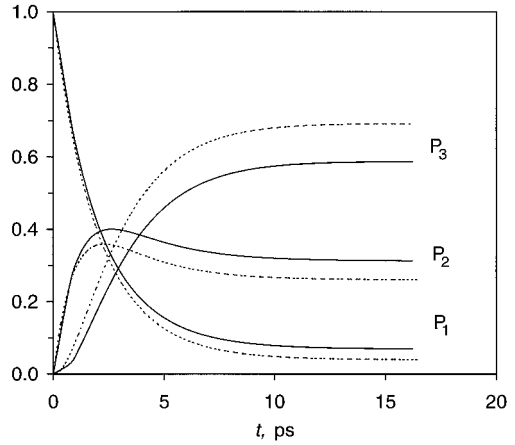

Figure 8. Evolution of the electronic state populations for mutant M1 with the parameters $E_2 = -400$ cm^{-1}, $E_3 = -630$ cm^{-1}, and $V_{12} = V_{23} = 22$ cm^{-1}. The solvation energy of the initial state is $E_s = 500$ cm^{-1} ($\delta = 1$). Dashed and solid lines correspond to SD1 and SD2, respectively. All results shown are converged to 5%.

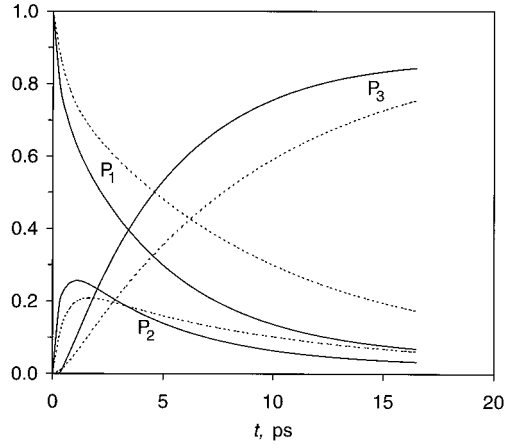

Figure 9. Evolution of the electronic state populations for mutant M1 with the parameters $E_2 = +200$ cm^{-1}, $E_3 = -630$ cm^{-1}, and $V_{12} = V_{23} = 30$ cm^{-1}. The solvation energy of the initial state is $E_s = 500$ cm^{-1} ($\delta = 1$). Dashed and solid lines correspond to SD1 and SD2, respectively. All results shown are converged to 5%.

placed the primary electron acceptor by a bacteriochlorophyll and studied the electron transfer rate in the resulting so-called β mutant.[58] Zinth and co-workers have reported substantial ($\sim$0.3) long-lived population of the accessory bacteriochlorophyll in a modified species (reaction center M1) where the bacteriopheophytin was replaced by a pheophytin whose free energy is estimated to be only 630 cm^{-1} lower than that of the excited special pair. (Extinction coefficients of the contributing pigment molecules are not reported in ref 12). Similar observations have been reported on a species containing 3-vinylbacteriopheophytin.[13] This population, which is sustained for more than 100 ps, is depleted slowly over a time scale that corresponds to electron transfer to the primary quinone.[12]

As discussed in our earlier work, these observations, along with accurate fully quantum mechanical simulations, lead to unambiguous determination of the charge transfer mechanism. The observation of electron transfer in ref 58 implies that the free energy of the reduced bacteriochlorophyll acceptor and, to a first approximation, that of the bridge is lower than that of the donor. Further, agreement with the experimental finding of Schmidt *et al.*[12] is possible only if the bridge free energy lies within a narrow range around 400 cm^{-1} below the free energy of the excited special pair. This value, which agrees with that proposed by Schmidt *et al*. on the basis of kinetic fits to their data, leads to a long-time bridge population of about 0.3, in fairly close agreement with the one-dimensional thermodynamic estimate (within the three-state model) at 300 K. As the substitution of the acceptor chromophore is not expected to affect the donor−bridge coupling significantly, the value of V_{12} is kept equal to 22 cm^{-1} in the simulations. On the other hand, the above substitution does affect the bridge−acceptor coupling strength. We find that the population characteristics are largely insensitive to the value of this coupling as long as $V_{23} \geq V_{12}$. Thus, our dynamics calculations alone cannot determine the value of the bridge−acceptor coupling in these mutants. Figure 8 shows the calculated populations with $E_2 = -400$ cm^{-1} and $E_s = 500$ cm^{-1} for the simple choice $V_{23} = V_{12} = 22$ cm^{-1} (configuration C3). These results are in very good agreement with the data and kinetic fit reported by Zinth's group. The other modified reaction centers mentioned earlier in this section, in which the acceptor free energy is raised with respect to that of the native species, exhibit qualitatively similar population dynamics in our simulations, in general agreement with the experimental observations. However, modification of the acceptor free energy and the bridge−acceptor coupling alone

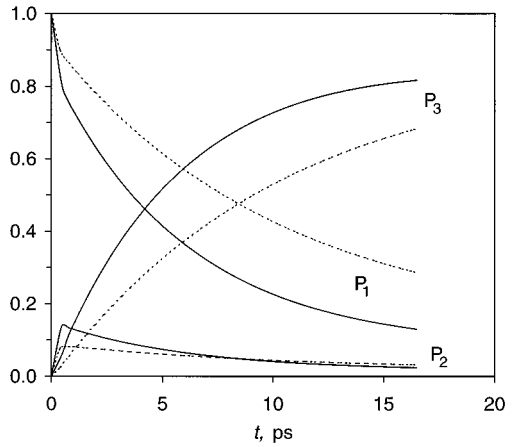

Figure 10. Evolution of the electronic state populations for mutant M1 with the parameters $E_2 = +500$ cm^{-1}, $E_3 = -630$ cm^{-1}, and $V_{12} = V_{23} = 60$ cm^{-1}. Dashed and solid lines correspond to SD1 and SD2, respectively. The solvation energy of the initial state is $E_s = 500$ cm^{-1} ($\delta = 1$). All results shown are converged to 5%.

cannot account for the approximately 2-fold increase of the kinetic constant observed in some of these systems.[58,13] It has been argued[13] that the presence of polar groups in the chemically modified reaction centers, which perturb the free energy of the bacteriochlorophyll intermediate, is largely responsible for this effect.

Values of the free energy much higher than -400 cm^{-1} can still give rise to considerable transient population if the initial excess energy of the medium (i.e., the reorganization energy for the P $\rightarrow$ P* transition) is significant. However, this population rapidly decays to its equilibrium value, which is nearly zero if $E_2 > 0$. Typical simulation results with configurations C3−C6 and $E_s = 500$ cm^{-1} are shown in Figures 9−11 for both spectral densities. With large positive values of E_2 the dominant mechanism is superexchange and the electronic couplings must be large in order to yield the observed 3 ps charge transfer. In this case the FPF scheme requires large numbers of paths and quantitative convergence become difficult. Moreover, essentially no population is observed on the accessory chlorophyll for $E_2 > 500$ cm^{-1}. The noticeable transient bridge population seen in the case of SD2 when $0 < E_2 \leq E_s$ arises from the slow relaxation of the medium from its initial nonequilibrium configuration. This transient population becomes smaller if the initial state is displaced by smaller amounts

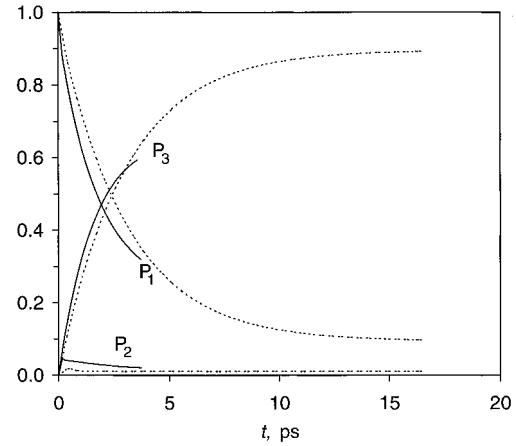

Figure 11. Evolution of the electronic state populations for mutant M1 with the parameters $E_2 = +2000$ cm^{-1}, $E_3 = -630$ cm^{-1}, and $V_{12} = V_{23} = 240$ cm^{-1}. Dashed and solid lines correspond to SD1 and SD2, respectively. The solvation energy of the initial state is $E_s = 500$ cm^{-1} ($\delta = 1$). All results shown are converged to 5%.

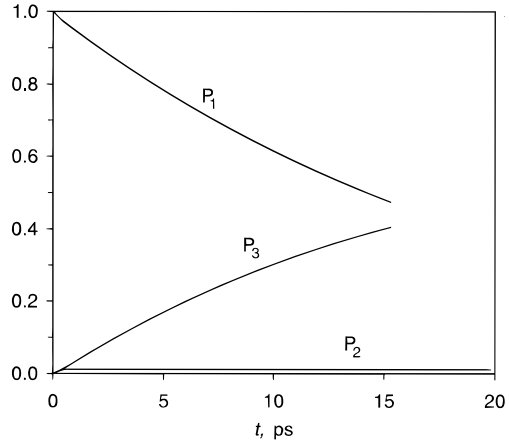

Figure 12. Evolution of the electronic state populations for mutant M2 using SD1 with the parameters $E_2 = +500$ cm^{-1}, $E_3 = -400$ cm^{-1}, and $V_{12} = 22$ cm^{-1}, and $V_{23} = 135$ cm^{-1}. The solvation energy of the initial state is $E_s = 500$ cm^{-1} ($\delta = 1$). The results shown are converged to 10%.

from its equilibrium configuration. With high-lying bridge configurations, significant population of the reduced accessory bacteriochlorophyll would be possible only if the corresponding electronic coupling were sufficiently large to mix this state with the donor, i.e., if $V_2 \approx E_2$; clearly, electronic couplings on the order of thousands of wavenumbers are extremely unlikely.

From the above we conclude that the detection of a long-lived intermediate reported by Zinth's group implies a low-lying reduced accessory bacteriochlorophyll with $E_2 \approx -400$ cm^{-1}. By virtue of the identical chemical structure of the donor and bridge states of this mutant with those of the native species, this conclusion carries over (at least approximately) to the wild-type reaction center. Combined with the room-temperature kinetic constants obtained by Martin and co-workers,[6−8] our simulations lead to approximate determination of (or a lower bound on) all energy parameters entering the Hamiltonian of eq 2.1 in the native reaction center.

3. Double Mutant. Holten and co-workers have studied a double mutant[56] where an aspartic acid is introduced near ring V of B_L in a *Rhodobacter capsulatus* in which H_L is also replaced by B_L (reaction center M2). These authors speculated on the basis of other evidence that the possibly charged character of the Asp residue leads to a significant (>800 cm^{-1}) increase of the bridge free energy from its native value.[56] With these energetic characteristics mutant M2 exhibits a slower primary electron transfer to the L-side chromophores with kinetic constant ~21 ps and a somewhat reduced quantum yield due to competing deactivation to the ground state and transfer to the M side of the polypeptide.[56]

We have calculated the electron transfer dynamics with free energies modified according to the arguments presented above. The electronic structure calculations of Zhang and Friesner[33] showed that the interstate couplings are insensitive to the specific modifications introduced to the wild-type reaction center by Holten's group. We thus used the wild-type optimized values $V_{12} = 22$ cm^{-1}, $V_{23} = 135$ cm^{-1} in the simulation of the double mutant (configuration C7). The simulation results are shown in Figure 12 for $E_s = 500$ cm^{-1} and spectral density SD1. It is seen that the changes in the energetics induced by the chemical modification of Heller *et al.*[56] lead to slower kinetics. Specifically, the time constant for the primary charge transfer in the double mutant is increased to 20 ps, in excellent agreement with the kinetic data of ref 56.

B. Temperature Dependence of Charge Transfer Rate. Fleming *et al.* have probed the temperature dependence of the electron transfer rate in the reaction centers of various photosynthetic bacteria.[5,9,10] These experiments have revealed a weak inverse temperature effect, with the rate increasing by a factor of 2−4 when the temperature is lowered from 300 to 10 K.

Clearly, there are several factors controlling this temperature variation that cannot be captured within the simplified three-state model considered in this article. First, the thermal contraction of the protein at low temperatures probably leads to an increase of the electronic couplings, thus facilitating transfer. Second, freezing affects the spectral density and also introduces glassy behavior, which may lead to deviations from simple Gaussian both dynamics; in addition, the reorganization energy may appear to be temperature-dependent below the glass transition.[57]

We have examined the temperature dependence of the rate arising from our model with the optimal wild-type parameters determined in the first part of this section. In the absence of more specific information the free energies, electronic couplings, and spectral densities remain fixed in our simulations while the temperature is lowered to 40 K. As seen in Figure 13, there is essentially no temperature variation of the electron transer rate in our model. The temperature independence of the electron transfer rate is primarily due to the nearly activationless intersection of the diabatic potential curves corresponding to the rate-determining first electron transfer step. At low temperatures this effect is further aided by the unrelaxed character of the initial protein configuration assumed in these simulations as well as the strongly quantum mechanical character of the medium, which leads to tunneling contributions. The absence of a temperature effect in our simulations is completely in accord with well-known results for the standard spin-boson model.[45] It is therefore not necessary to invoke a superexchange contribution to the primary charge separation in order to account for the lack of a strong sensitivity of this process to environmental conditions. Given that our simplified three-state model ignores other temperature-dependent factors alluded to above, we consider the obtained agreement with the experimental temperature dependence of the charge transfer rate to be sufficiently satisfactory.

The same lack of sensitivity to external temperature is observed in Figure 14, which shows our simulations of the modified reaction center M1 with the optimal configuration C3, in which the rate-determining first kinetic step involves the same two-state configuration as the native species. By contrast, a strong temperature dependence should be observable in this

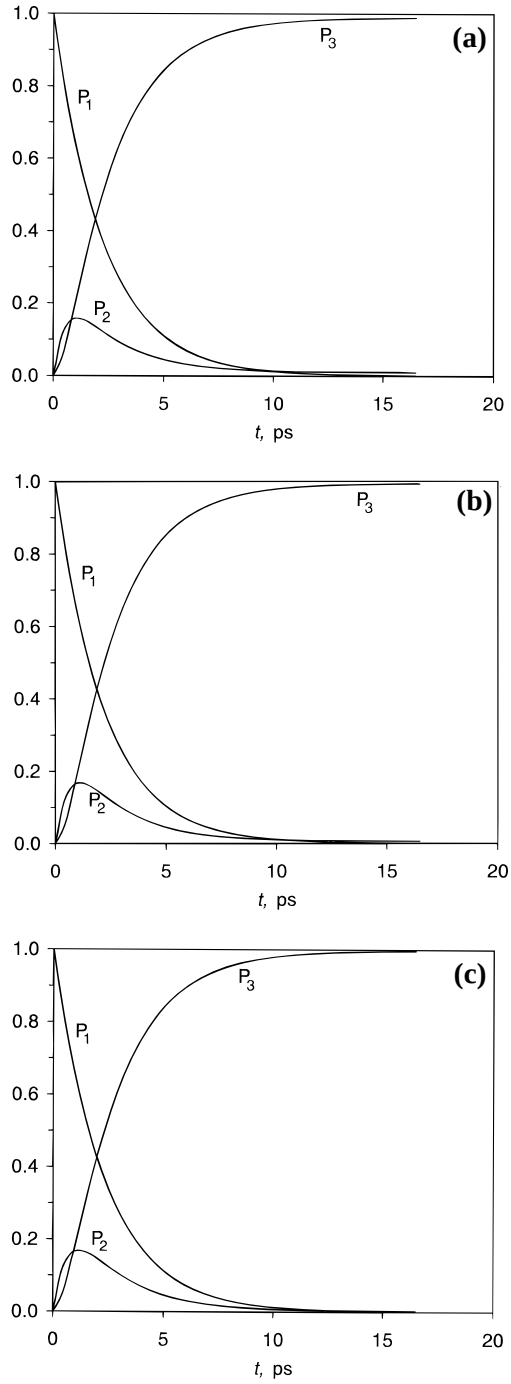

Figure 13. Comparison of the calculated kinetics of primary charge separation in the wild-type reaction center with spectral density SD1 and the parameters $E_2 = -400$ cm^{-1}, $E_3 = -2000$ cm^{-1}, $V_{12} = 22$ cm^{-1}, and $V_{23} = 135$ cm^{-1} at three different temperatures. The solvation energy of the initial state is $E_s = 500$ cm^{-1} ($\delta = 1$). All results shown are converged to 2%. (a) $T = 280$ K. (b) $T = 160$ K. (c) $T = 40$ K.

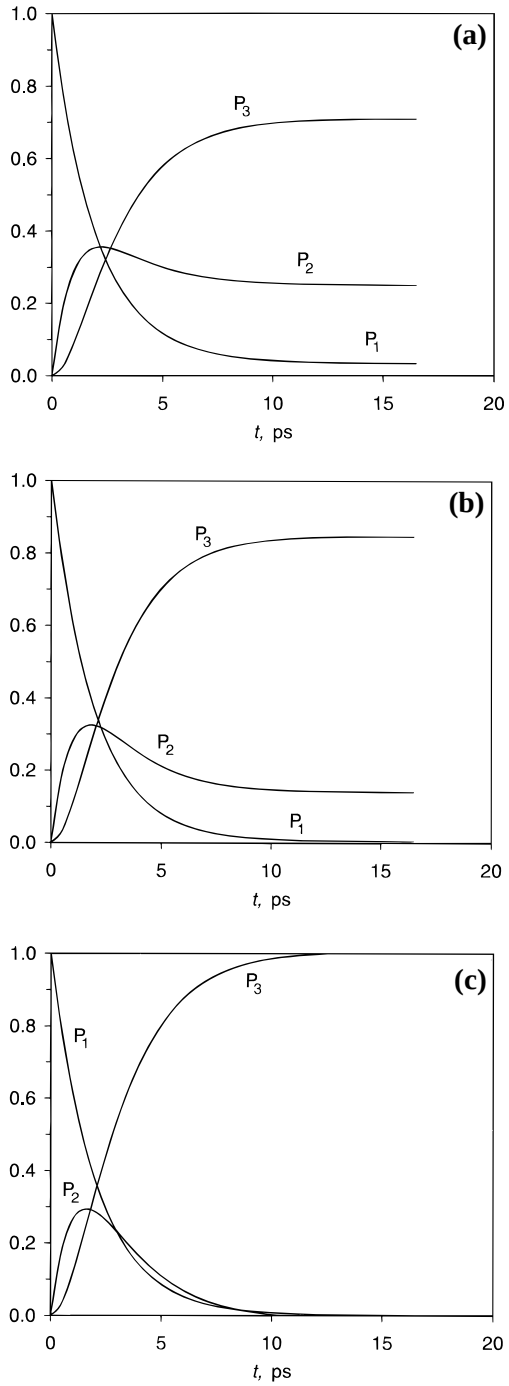

Figure 14. Comparison of the calculated kinetics of primary charge separation in modified reaction center M1 with spectral density SD1 and the parameters $E_2 = -400$ cm^{-1}, $E_3 = -630$ cm^{-1}, and $V_{12} = V_{23} = 22$ cm^{-1} at three different temperatures. The solvation energy of the initial state is $E_s = 500$ cm^{-1} ($\delta = 1$). All results shown are converged to 2%. (a) $T = 280$ K. (b) $T = 160$ K. (c) $T = 40$ K.

system if a superexchange mechanism is operative with a large donor−bridge energy gap, as a consequence of a sizable activation factor between donor and acceptor states in this species. Indeed, Figure 15 shows a dramatic deceleration of the electron transfer dynamics at $T = 160$ K with configuration C5, which assumes a bridge free energy equal to 500 cm^{-1}. Kinetic experiments by Kirmaier *et al.*[58] on the β mutant, which contains the same donor and bridge units as the native reaction center, report a weak temperature effect and thus are consistent with the results of our simulations that employ the optimal bridge free energy $E_2 = -400$ cm^{-1}. Experimental determination of the temperature dependence of the primary charge separation rate in the modified reaction center M1 and also in the high-bridge double mutant should offer additional evidence in this regard.

C. Dependence of Simulation Results on Initial Preparation. Generally, we find that the electronic population dynamics presented above are qualitatively insensitive to reasonable variations of the configuration and excess energy of the nonequilibrium initial state of the excited special pair. In the case of SD1, where the medium relaxation is fast compared to the time scale of electron transfer, the dependence of the kinetics on the initial solvation energy is negligible. This behavior is illustrated in Figure 16, where the decay rates of the excited

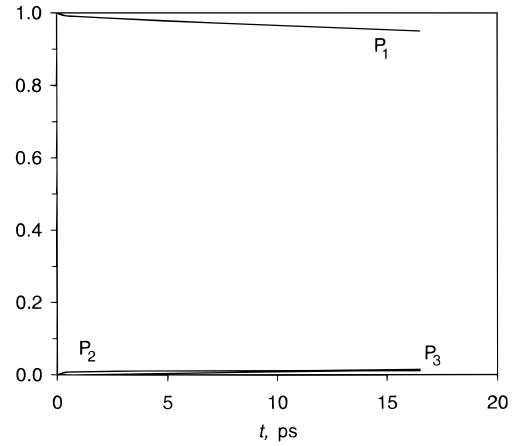

Figure 15. Electronic state populations for mutant M1 at $T = 160$ K obtained with SD1 assuming a high-energy bridge (configuration C5, $E_2 = +500$ cm^{-1}) for which electron transfer evolves primarily via superexchange. The solvation energy of the initial state is $E_s = 500$ cm^{-1} ($\delta = 1$). All results shown are converged to 5%.

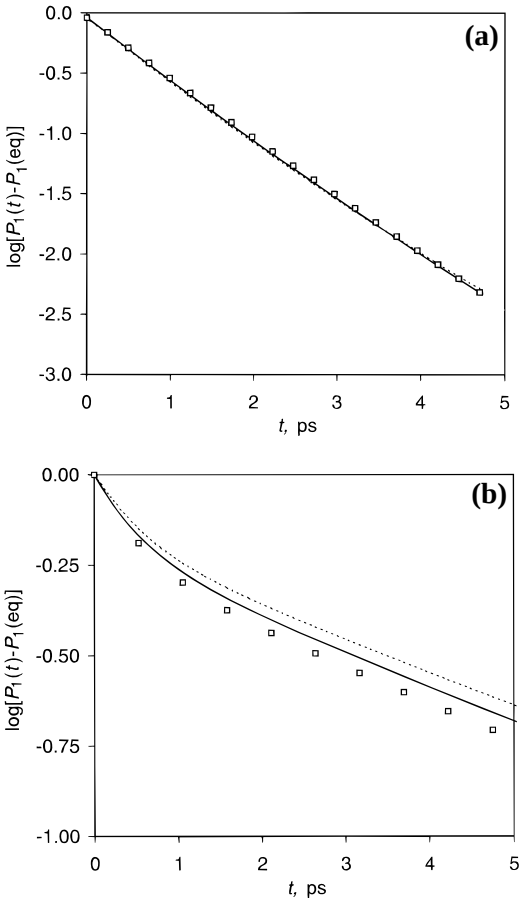

Figure 16. Effects of initial state characteristics on the electron transfer dynamics in mutant M1 calculated with SD1 for two bridge configurations. Shown is the logarithm of the donor population with respect to its equilibrium value as a function of time. The electronic populations are converged to 2%. Solid line: $E_s = 0$. Markers: $E_s = 500$ cm^{-1}, $\delta = 1$ (initial state displaced toward the bridge). Dashed line: $E_s = 500$ cm^{-1}, $\delta = -1$ (initial state displaced away from the bridge). (a) $E_2 = -400$ cm^{-1} (configuration C3). (b) $E_2 = +200$ cm^{-1} (configuration C4).

special pair in mutant M1 that correspond to $E_s = 500$ (with $\delta = \pm 1$) or 0 cm^{-1} ($\delta = 0$) are compared for the configurations C3 and C4. On the other hand, somewhat more significant initial state effects are observed if the lower frequency SD2 is used. As the time scales for protein relaxation and initiation

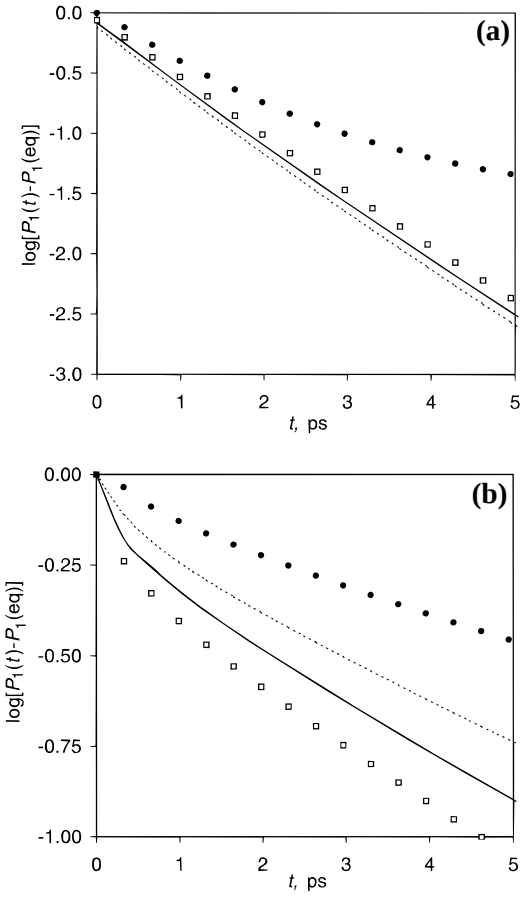

Figure 17. Effects of initial state characteristics on the electron transfer dynamics in mutant M1 calculated with SD1 for two bridge configurations. Shown is the logarithm of the donor population with respect to its equilibrium value as a function of time. The electronic populations are converged to 5%. Dashed line: $E_s = 0$. Solid line: $E_s = 125$ cm^{-1}, $\delta = 1/2$. Hollow squares: $E_s = 500$ cm^{-1}, $\delta = 1$ (initial state displaced toward the bridge). Filled circles: $E_s = 500$ cm^{-1}, $\delta = -1$ (initial state displaced away from the bridge). (a) $E_2 = -400$ cm^{-1} (configuration C3). (b) $E_2 = +200$ cm^{-1} (configuration C4).

of electron transfer are not very dissimilar in this case, displacement of the initial state toward the point of crossing with the accessory bacteriochlorphyll generally enhances the first step of the electron transfer process.[43] This behavior is illustrated in Figure 17, which shows the decay rate of the donor corresponding to different initial preparations for the optimal bridge parameters of configuration C3 as well as in the case of a higher lying bridge characterized by configuration C4. Initial states displaced toward the bridge lead to enhancement of the rate in the case of configuration C4, which is characterized by substantial activation energy. With the optimal bridge free energy $E_2 = -400$ cm^{-1}, which corresponds to a nearly activationless crossing of the donor and bridge states, the early stages of charge transfer appear rather insensitive to the precise form of the initial state of the medium. We therefore conclude that our proposal of 22 cm^{-1} for the donor−bridge coupling is reliable.

V. Discussion and Concluding Remarks

By comparing the results of rigorous quantum dynamical simulations for a simple dissipative three-state model of the pigment molecules in bacterial reaction centers to available experimental data, we have estimated the bridge free energy and electronic couplings responsible for primary charge separation. For wild-type reaction centers, the optimized values that we determined correspond to a reduced accessory bacteriochlo-

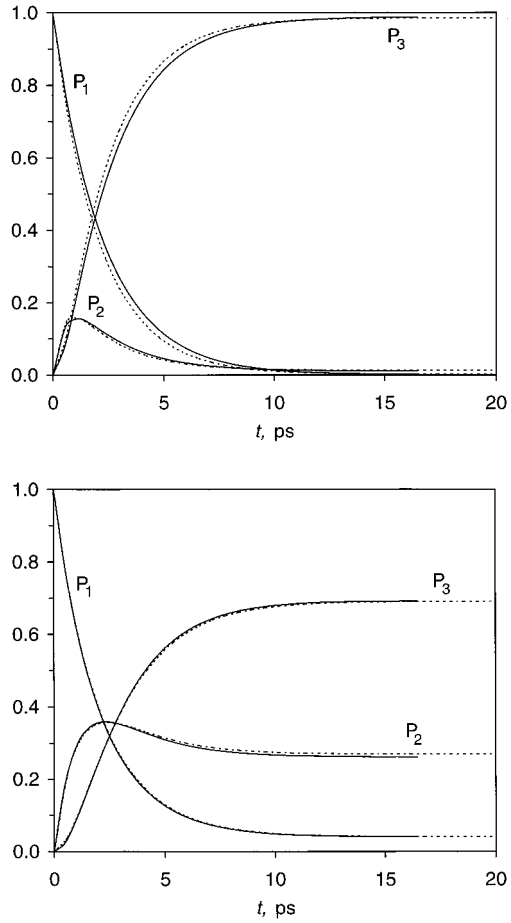

Figure 18. Comparison between the quantum path integral simulation results (solid lines) and the two-step kinetic equation results (dashed lines) with the optimal bridge free energy $E_2 = -400$ cm^{-1} and spectral density SD1 at 300 K. (a) Wild-type reaction center (configuration C2). (b) Mutant M1 (configuration C3).

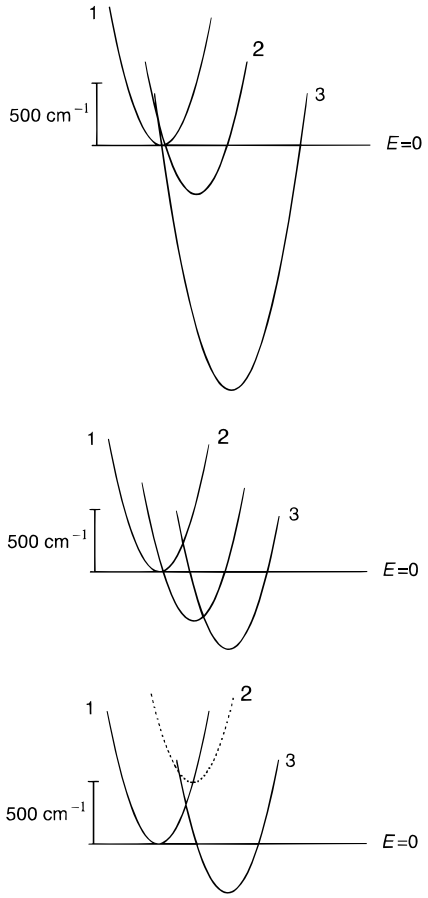

Figure 19. Schematic representation of the diabatic surfaces corresponding to the bacteriochlorophyll special pair, the reduced bacteriochlorophyll monomer, and the reduced bacteriopheophytin with the optimal parameters deduced from our simulations. (a) Wild-type reaction center. (b) Zinth's modified reaction center. (c) Holten's double mutant. The dashed line in Figure 19c indicates a significant uncertainty with respect to the free energy of that state.

rophyll that lies about 400 cm^{-1} below the excited special pair, while the donor−bridge and bridge−acceptor electronic couplings are estimated to be 22 and $\geq$135 cm^{-1}, respectively. The temperature dependence of the electron transfer rate predicted from our model with these optimized parameters, as well as its variation in response to chemical modifications of the chromophores, is in very good agreement with the results of time-resolved experiments on these systems. Recent *ab initio* electronic structure calculations obtained values for the electronic couplings that are in accord with our dynamics-based estimates.

The above estimated values of the bridge free energy and electronic couplings imply that the primary charge separation is a two-step process, in harmony with the theoretical analysis of Marcus.[17,18] To verify this conclusion, we have compared the full three-state simulation results with those obtained from the two coupled kinetic equations

$$P^*B_L\,H_L \underset{k_{-1}}{\overset{k_1}{\rightleftharpoons}} P^{*+}B_L^-\,H_L \underset{k_{-2}}{\overset{k_2}{\rightleftharpoons}} P^{*+}B_L\,H_L^- \qquad (5.1)$$

where the single-step rates are obtained from path integral calculations on the individual two-state subsystems in the cases of the wild-type reaction center and of mutant M1 calculated with SD1 at room temperature. As seen in Figure 18, the fit between these results is excellent. While the rate-determining step is the donor-to-bridge transfer, a relatively large value of the kinetic constant for the second step explains the absence of the accessory chlorophyll from the recorded absorption spectra within the detection threshold of time-resolved experiments on wild-type reaction centers. Detection of that state in the modified species studied by Zinth and co-workers is primarily a consequence of favorable thermodynamic factors.

The free energy surfaces arising from these optimized parameters are shown in Figure 19 for the three systems studied here. The nearly activationless crossing of the free energy surfaces in the native reaction center and in those with modified acceptor pigments accounts for the insensitivity of the observed kinetics to large temperature variations. For the same reason, our simulation results as well as our estimate of the donor−bridge coupling are largely insensitive to assumed details of the model and thus (to the extent that the harmonic description of the protein environment is valid) sufficiently reliable.

Acknowledgment. We are happy to acknowledge fruitful discussions with Professors David Chandler, Richard Friesner, Jose Onuchic, and Peter Wolynes. We also thank Professors Dewey Holten, Mark Ratner, and Arieh Warshel for useful comments on the manuscript. This work has been supported by the National Science Foundation through a Young Investigator Award.

References and Notes

(1) Deisenhofer, J.; Epp, O.; Miki, K.; Huber, R.; Michel, H. *J. Mol. Biol.* **1984**, *180*, 385−398.

(2) Deisenhofer, J., Norris, J. R., Eds.; Academic Press: New York, 1993; Vol. 2.

(3) Fleming, G. R.; Grondelle, R. V. *Phys. Today* **1994**, *Feb.*, 49−55.
(4) Holten, D.; Hoganson, C.; Windsor, M. W.; Schenck, C. C.; Parsons, W. W.; Migus, A.; Fork, R. L.; Shank, C. V. *Biochim. Biophys. Acta* **1980**, *592*, 461−477.
(5) Woodbury, N. W.; Becker, M.; Middendorf, D.; Parson, W. W. *Biochemistry* **1985**, *24*, 7516−7521.
(6) Martin, J.-L.; Breton, J.; Hoff, A. J.; Migus, A.; Antonetti, A. *Proc. Natl. Acad. Sci. U.S.A.* **1986**, *83*, 957−961.
(7) Breton, J.; Martin, J. L.; Migus, A.; Antonetti, A.; Orszag, A. *Proc. Natl. Acad. Sci. U.S.A.* **1986**, *83*, 5121−5125.
(8) Breton, J.; Martin, J. L.; Petrich, J.; Migus, A.; Antonetti, A. *FEBS Lett.* **1986**, *209*, 37−43.
(9) Breton, J.; Martin, J.-L.; Fleming, G. R.; Lambry, J.-C. *Biochemistry* **1988**, *27*, 9276−9284.
(10) Fleming, G. R.; Martin, J. L.; Breton, J. *Nature (London)* **1988**, *333*, 190−192.
(11) Chan, C.-K.; DiMagno, T. J.; Chen, L. X.-Q.; Norris, J. R.; Fleming, G. R. *Proc. Natl. Acad. Sci. U.S.A.* **1991**, *88*, 11202−11206.
(12) Schmidt, S.; Arlt, T.; Hamm, P.; Huber, H.; Nagele, T.; Wachtevitl, J.; Meyer, M.; Scheer, H.; Zinth, W. *Chem. Phys. Lett.* **1994**, *223*, 116−120.
(13) Huber, H.; Meyer, M.; Nagele, T.; Hartl, I.; Scheer, H.; Zinth, W.; Wachtveitl, J. *Chem. Phys.* **1995**, *197*, 297−305.
(14) Egger, R.; Mak, C. H.; Weiss, U. *Phys. Rev. E* **1994**, *50*, R655−R658.
(15) Bixon, M.; Jortner, J.; Michel-Beyerle, M. E.; Ogrodnik, A.; Lersch, W. *Chem. Phys. Lett.* **1987**, *140*, 626−630.
(16) Bixon, M.; Jortner, J.; Michel-Beyerle, M. E. *Biochim. Biophys. Acta* **1991**, *1056*, 301−315.
(17) Marcus, R. A. *Chem. Phys. Lett.* **1987**, *133*, 471−477.
(18) Marcus, R. A. *Chem. Phys. Lett.* **1988**, *146*, 13−21.
(19) Parson, W. W.; Creighton, S.; Warshel, A. In *Primary Processes in Photobiology*; Kobayashi, T., Ed.; Springer-Verlag: Berlin, 1987.
(20) Warshel, A.; Creighton, S.; Parson, W. W. *J. Phys. Chem.* **1988**, *92*, 2696−2701.
(21) Creighton, S.; Hwang, J. K.; Warshel, E.; Parson, W. W.; Norris, J. *Biochemistry* **1988**, *27*, 774−781.
(22) Sharp, K.; Honig, B. *Annu. Rev. Biophys. Biophys. Chem.* **1990**, *19*, 301−332.
(23) Thompson, M. A.; Zerner, M. C. *J. Am. Chem. Soc.* **1991**, *113*, 8210−8215.
(24) Marchi, M.; Gehlen, J. N.; Chandler, D.; Newton, M. *J. Am. Chem. Soc.* **1993**, *115*, 4178−4190.
(25) Alden, R. G.; Parson, W. W.; Chu, Z. T.; Warshel, A. *J. Am. Chem. Soc.* **1995**, *117*, 12284−12298.
(26) Hu, Y.; Mukamel, S. *J. Chem. Phys.* **1989**, *91*, 6973−6988.
(27) Hu, Y.; Mukamel, S. *Chem. Phys. Lett.* **1989**, *160*, 410−416.
(28) Egger, R.; Mak, C. H. *J. Phys. Chem.* **1994**, *98*, 9903−9918.
(29) Mak, C. H.; Egger, R. *Chem. Phys. Lett.* **1995**, *238*, 149−157.
(30) Makri, N.; Sim, E.; Makarov, D. E.; Topaler, M. *Proc. Natl. Acad. Sci. U.S.A.* **1996**, *93*, 3926−3931.
(31) Sim, E.; Makri, N. *Chem. Phys. Lett.* **1996**, *249*, 224−230.
(32) Sim, E.; Makri, N. *Comput. Phys. Commun.* **1997**, *99*, 335−354.
(33) Zhang, L. Y.; Friesner, R. A. *Proc. Natl. Acad. Sci. U.S.A.*, submitted.
(34) Makarov, D. E.; Makri, N. *Chem. Phys. Lett.* **1994**, *221*, 482.
(35) Marcus, R. A. *J. Chem. Phys.* **1956**, *24*, 966−978.
(36) Feynman, R. P.; Hibbs, A. R. *Quantum Mechanics and Path Integrals*; Mcraw-Hill: New York, 1965.
(37) Marcus, R. A.; Sutin, N. *Biochim. Biophys. Acta* **1985**, *811*, 265−322.
(38) Onuchi, J. N.; Wolynes, P. G. *J. Phys. Chem.* **1988**, *92*, 6495−6503.
(39) Onuchi, J. N.; Wolynes, P. G. *J. Phys. Chem.* **1993**, *98*, 2218−2224.
(40) Marcus, R. A. *Angew. Chem., Int. Ed. Engl.* **1993**, *32*, 1111−1121.
(41) Warshel, A.; Hwang, J.-K. *J. Chem. Phys.* **1986**, *84*, 4938−4957.
(42) Warshel, A.; Chu, Z. T.; Parson, W. W. *Science* **1989**, *246*, 112−116.
(43) Cho, M.; Silbey, R. *J. Chem. Phys.* **1995**, *103*, 595−606.
(44) Feynman, R. P.; F. L. Vernon, J. *Ann. Phys.* **1963**, *24*, 118−173.
(45) Leggett, A. J.; Chakravarty, S.; Dorsey, A. T.; Fisher, M. P. A.; Garg, A.; Zwerger, M. *Rev. Mod. Phys.* **1987**, *59*, 1−85.
(46) Goldstein, R. A.; Takiff, L.; Box, S. G. *Biochim. Biophys. Acta* **1988**, *934*, 253−263.
(47) Chidsey, C. E. D.; Takiff, L.; Goldstein, R. A.; Boxer, S. G. *Proc. Natl. Acad. Sci. U.S.A.* **1985**, *82*, 6850−6854.
(48) Leguit, L.; Visschers, R. W.; Crielaard, W.; Grondelle, R. v.; Hellingwerf, K. J. *Biochim. Biophys. Acta* **1992**, *1102*, 177−185.
(49) Schulten, K.; Tesch, M. *Chem. Phys.* **1991**, *158*, 421−446.
(50) Gehlen, J. N. Ph.D. Thesis, University of California, 1994.
(51) Gehlen, J.; Marchi, M.; Chandler, D. *Science* **1994**, *263*, 499−502.
(52) Makri, N.; Makarov, D. E. *J. Chem. Phys.* **1995**, *102*, 4611.
(53) Makri, N. *J. Math. Phys.* **1995**, *36*, 2430−2456.
(54) Makri, N. Path integral simulation of long-time dynamics in quantum dissipative systems. In *Path integrals: Basics and Applications*; DeWitt-Morette, C., Ed.; Plenum, New York, 1997.
(55) Makri, N. *Chem. Phys. Lett.* **1992**, *193*, 435.
(56) Heller, B. A.; Holten, D.; Kirmaier, C. *Science* **1995**, *269*, 940−945.
(57) Hoffman, B. M.; Ratner, M. A. *Inorg. Chim. Acta* **1996**, *243*, 233−238.
(58) Kirmaier, C.; Laporte, L.; Schenck, C. C.; Holten, D. *J. Phys. Chem.* **1995**, *99*, 8910.
(59) Warshel, A.; Parson, W. W. *Annu. Rev. Phys. Chem.* **1991**, *42*, 279.
(60) Alden, R. G.; Parson, W. W.; Chu, Z. T.; Warshel, A. *J. Am. Chem. Soc.* **1995**, *117*, 12284.